IR susceptibility of naval ships using ShipIR/NTCS

David A. Vaitekunas[a,1]
[a]W.R. Davis Engineering Limited, 1260 Old Innes Road, Ottawa, Ontario, Canada K1B 3V3

Presented at the SPIE Defence, Security, and Sensing, Orlando, Florida, USA, 5-9 April, 2010 (Paper no. 7662-31)

ABSTRACT

Methods of analysing the signature and susceptibility of naval platforms to infrared detection are described. An unclassified ShipIR destroyer model is used to illustrate the primary sources of infrared signature and detection: the exhaust system, solar-heating, and operating climate. The basic detection algorithm used by the Naval Threat Countermeasure Simulator (NTCS) component of ShipIR is described and used to analyse the effectiveness of various stealth technologies: stack suppression, low solar absorptive (LSA) paints, and Active Hull Cooling (AHC). Standard marine climate statistics are used to determine a minimum (5%), average (50%) and maximum (95%) signature condition for each operating region. The change in detection range of two wave-band sensors (3–5μm, 8–12 μm) operating at different altitudes (10m, 270m) in each of four climatic conditions is used to assess the effectiveness of each stealth solution, providing a more integral approach to infrared stealth design. These tools and methods form the basis on which future platform designs are being evaluated.

Keywords: infrared signature, infrared detection, ship model, numerical simulation, infrared stealth, effectiveness, suppression

2. INTRODUCTION

ShipIR/NTCS is a comprehensive software engineering tool for predicting the thermal infrared (IR) signature and IR susceptibility of naval warships. The ShipIR component consists of several sub-models, including the MODTRAN4 infrared sky radiance and atmosphere propagation model, a proprietary sea reflectance model combining the methods of Mermelstein (1994) with the results from Shaw and Churnside (1997) and Ross and Dion (2007). The platform model is created from a 3D surface geometry which forms the basis of both a radiative heat transfer and in-band surface radiance model comprised of both multi-bounce diffuse and specular reflections. An exhaust plume trajectory and IR emission model predicts the infrared signature of both diesel engine and gas turbine exhaust systems. Internal heat sources are modelled via user-defined thermal boundary conditions, simulating a complex thermal network of specified temperatures (controlled spaces), forced and natural convection conduits, heat-flux, and heat conduction. Validation of the ShipIR model has been the topic of numerous research papers (Vaitekunas and Fraedrich 1999, Fraedrich et al. 2003, Vaitekunas 2005).

In addition to providing basic image and polar signature analysis, Figure 1 illustrates how the infrared scenes produced by ShipIR are coupled with an imaging seeker and proportional navigation (P-N) algorithm to produce a closed-loop fly-in engagement analysis tool called the Naval Threat and Countermeasure Simulator (NTCS). Users provide their own seeker inputs (wave-band, field-of-view, array size) and detection criteria (noise/clutter threshold, signal-to-noise ratio, no. of pixels, no. of frames) to perform an IR susceptibility analysis. The software has already been used in the design of numerous warships (Spanish Frigate, New Norwegian Frigate, Korean KDX-III, Australian air warfare destroyer).

The unclassified ShipIR model of a destroyer shown in Figure 2 was created from a CAD model purchased on-line (http://www.turbosquid.com/3d) and will serve as a test article to illustrate the primary sources of infrared ship signature,

[1] dvaitekunas@davis-eng.com; http://www.davis-eng.com; phone: +1 613 748 5500; fax: +1 613 748 3972

demonstrate the methods used by NTCS to predict detection range, and show the benefits of various infrared signature suppression technologies. The propulsion and hotel power configurations to be simulated are shown in Table 1, and include three standard modes of operation: quiet (dw), cruise diesel (cr), and full-power gas turbine (fp). A dark-grey (α_s=0.90) and light-grey (α_s=0.50) version of the ship model is used to assess the benefits of using low solar absorptive (LSA) materials. Figures 3 and 4 show the real ship surface temperatures predicted by ShipIR for the sunlit and shaded sides of the light-grey destroyer, illustrating the variations that can occur over a large complex ship structure with many concave features. Figures 5 and 6 show a mid-wave and long-wave infrared image produced by ShipIR near the predicted detection range of 16.6km, demonstrating the relative significance of the exhaust plume emissions in the mid-wave IR band, versus the sun-heating and waterline in the long-wave IR band.

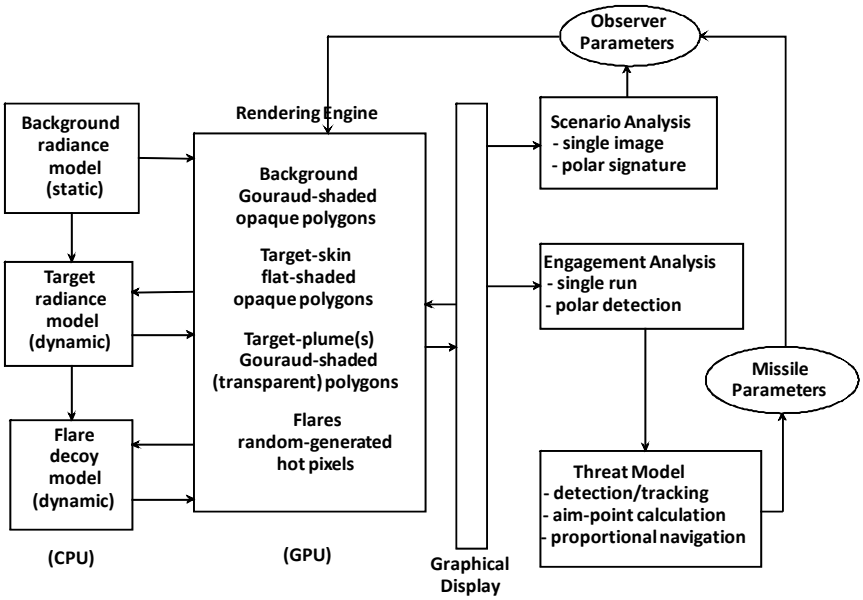

Figure 1: Scene generation architecture.

Apart from reducing the solar absorptivity of the paint (LSA), treatments to mitigate the risk of infrared detection include exhaust stack suppression and extension of the Fire / NBC (pre-wetting) system to operate as an active hull cooling (AHC) system. Figure 7 illustrates three of the most common stack suppression systems already in service. A passive Eductor/Diffuser offers the first line of defence against infrared detection by cooling both the exhaust gas and uptake metal of gas turbines, diesel engines, and diesel generators. The device mounts

Table 1: propulsion and hotel power configurations.

Modes	2 x MTU 20V956 TB92	2 x DN80 (Ukraine)	4 x MTU 16V396	Speed (kts)
dw			1.2 MW	0
cr	12.4 MW		2.5 MW	18
fp		43.4 MW	2.5 MW	29

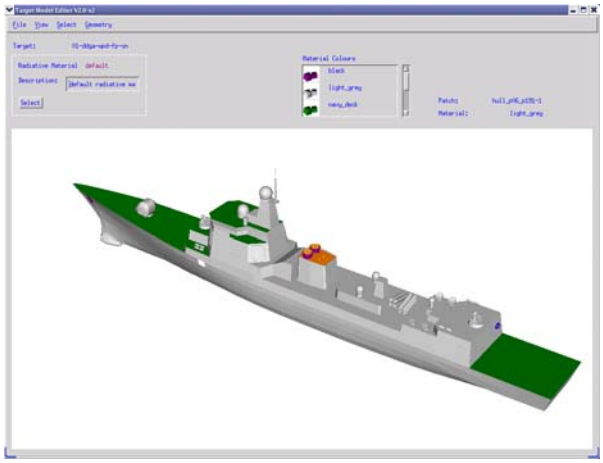

Figure 2: CAD model with light-grey paint schedule.

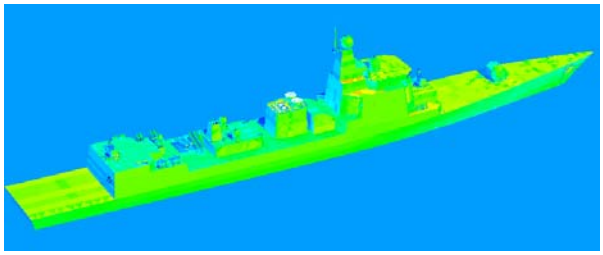

Figure 3: Real temperatures predicted by ShipIR on the sunlit side of the light-grey destroyer.

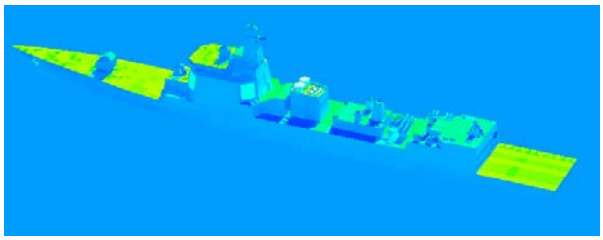

Figure 4: Real temperatures predicted by ShipIR on the shaded side of the light-grey destroyer.

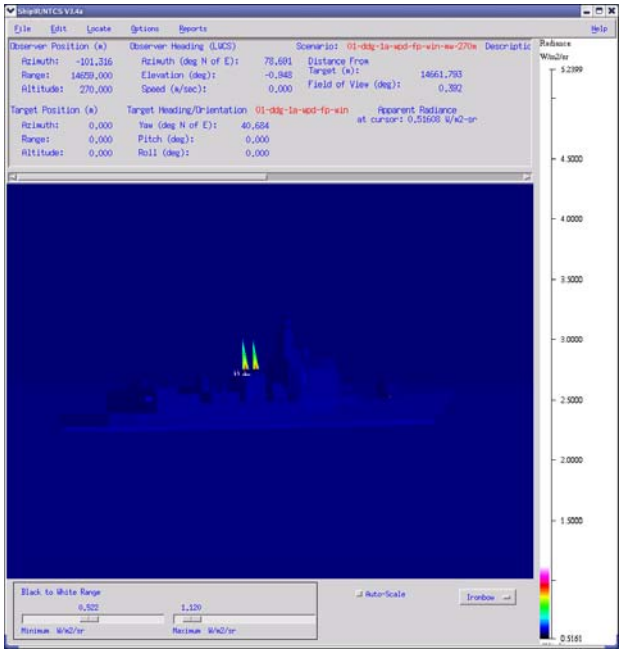

Figure 5: sample mid-wave (3-5 μm) image of destroyer.

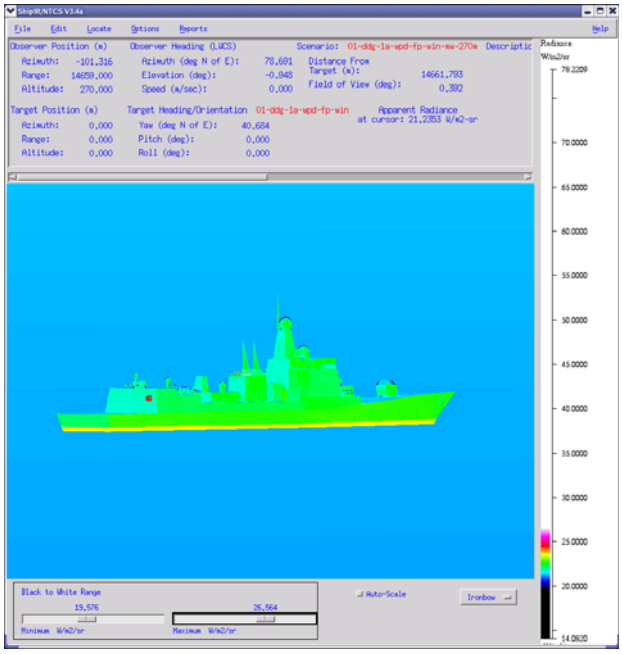

Figure 6: sample long-wave (8-12 μm) image of destroyer.

directly to the uptake and is normally fully enclosed inside the exhaust funnel. The uptake metal is cooled to within 25°C of the ambient air, and the plume temperature and exhaust constituents are typically diluted by about 50%. The Eductor/Diffuser consists of three components: an air-air ejector nozzle to pump the ambient air into the exhaust plume, a mixing tube to promote even distribution between the hot exhaust and cool ambient air, and a multi-ring diffuser to naturally entrain ambient air through the gaps between each ring to provide film cooling of the visible metal. Benefits of the Eductor/Diffuser include: Scalable to fit any size uptake, protection up to approximately 70° (from the horizontal), simple design for ease of integration, and no maintenance requirements. The DRES-Ball uses the same passive air-air ejector system as the Eductor/Diffuser, except the nozzle is formed by inserting a centre body which doubles as an optical block. Better mixing is also achieved by naturally entraining ambient air through the support struts at the base of the device and out through the film-cooled rings located on the visible portion of the centre body. Benefits of the DRES-Ball include: scalable to fit any size uptake, full hemispherical protection, more uniform plume temperature profile, best performance of all air-air suppressors, and no maintenance requirements. To achieve lower exhaust plume temperatures, a sea water Injection (SWI) system has been added to the passive Eductor/Diffuser. An array of atomizing nozzles inject a fine mist into the exhaust plume. As the water particles come into direct contact with the hot exhaust gas, heat is removed through the enthalpy of evaporation, resulting in a significant decrease in the gas temperature. Such systems are termed *active* because they are configured to only operate in high-threat scenarios, and they must interface with the ships machinery control system (MCS) to monitor and control the flow of water

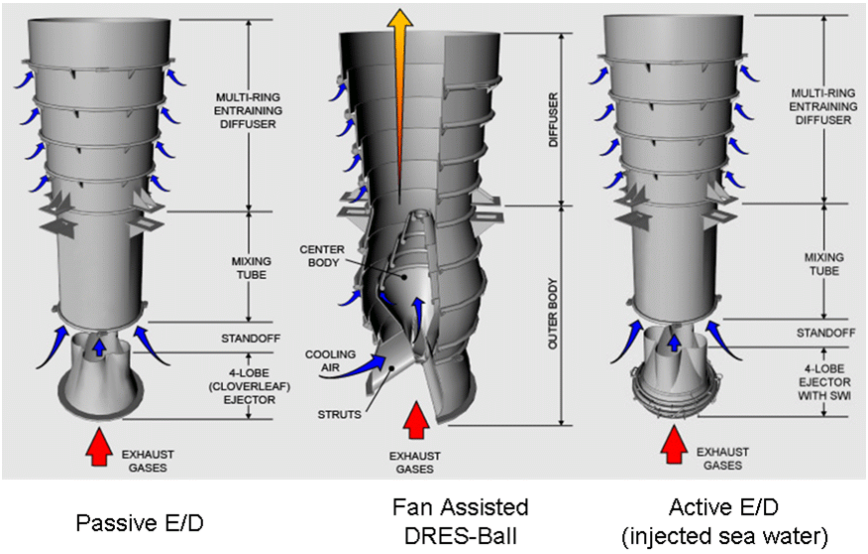

Figure 7: stack infrared suppression systems.

as a function of the engine power (exhaust heat). Benefits of sea water injection include: ability to deliver the same performance as a passive Eductor/Diffuser when not in use, custom nozzle selection and placement for optimal operating efficiency, and maximum IR suppressor performance.

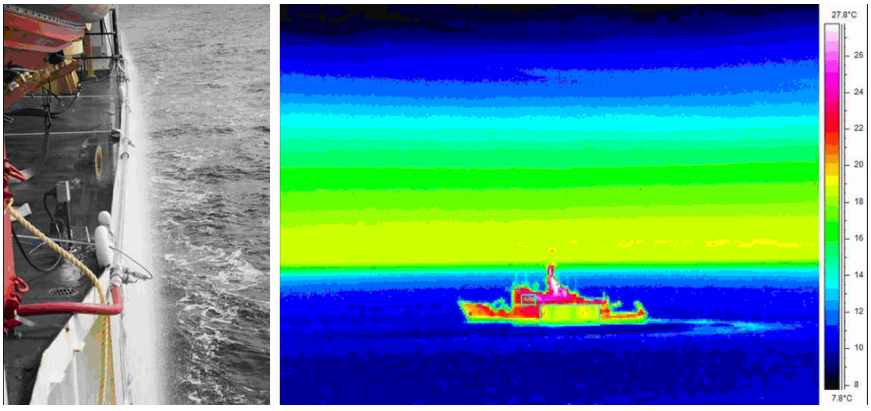

Figure 8: photograph and infrared image of an AHC system in use on the CFAV Quest.

Research and development has been underway for several years to study and model the thermal infrared properties of an active hull cooling (AHC) system, where temperature sensors installed on the inside surface of the ship hull and shipboard climatic sensors are used to monitor and control the hull skin signature. Figure 8 shows a visual and infrared image taken from the Onboard Signature Manager (OSM) currently installed on the Canadian Forces Auxiliary Vessel (CFAV) Quest, an unclassified Canadian Defence research vessel operated out of Halifax by the Canadian Navy and Defence Research Development Canada (Atlantic). Similar systems are now in service on the Spanish Frigate (F100), the New Norwegian Frigate (F310), and the new Korean KDX-III destroyer (DDG-110).

3. CLIMATIC ANALYSIS

The following methods are used to specify the climatic inputs to ShipIR. Monthly statistics on the average and standard deviation in sea temperature, air temperature, air-sea temperature difference (ASTD), dew-point, and wind speed are taken from the US Navy Marine Climatic Atlas of the World (US Naval Meteorology and Oceanography Command, 1995), and used to derive an accumulative probability for each variable in each month, as shown in Figures 9 through 11. A Normal distribution is assumed for all variables except wind speed. Low and moderate wind speeds tend to occur more often than gale force winds, therefore a 2-parameter (k,λ) Weibull distribution is used to fit the wind statistics for each month. The wind roses also taken from the US Marine Atlas are used to specify the predominant wind direction in each month. Taking the average accumulative probability from all twelve (12) months, a statistically significant minimum (5%), average (50%), and maximum (95%) value is computed for each climatic variable, along with the most likely month in which it occurs. Applying an equal weighting to all the input variables, the most likely month in which all five (5) variables attain their 5%, 50%, and 95% value is derived. These results are provided in Table 2 for the Eastern Sea (37°N, 133°E) located between Korea and Japan. The minimum value of all five input variables is expected to produce a maximum infrared signature: low humidity and air temperature maximize the solar-heating (visibility), infrared transmission, and gradients in sea / sky radiance; low wind speeds produce minimum convection, maximizing sun heating during the day, and minimizing air heating during the night. The air, sea and dew-point temperatures show a similar seasonal profile: minimum during the winter and maximum during the summer;

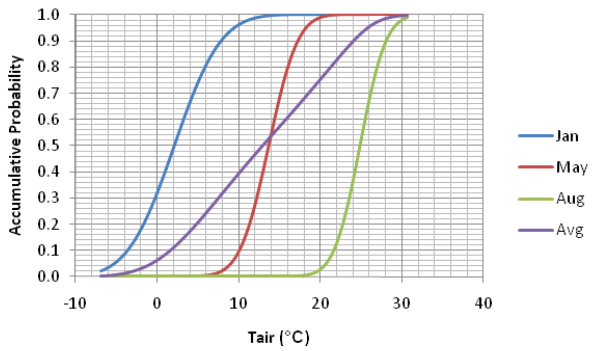

Figure 9: accumulative probabilities for air temperature.

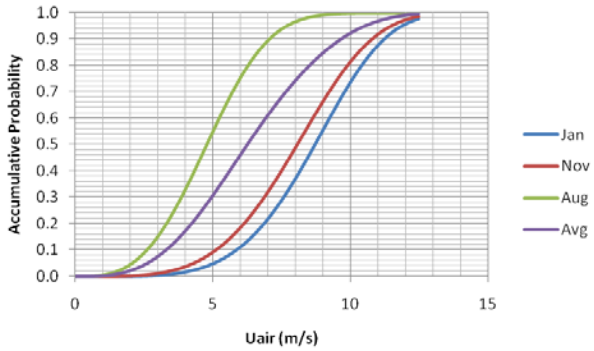

Figure 10: accumulative probabilities for wind speed.

whereas wind speed shows an opposite trend: increasing during the winter and decreasing during the summer. To resolve this discrepancy, the 5% value in the winter and the 95% value in the summer are used to specify the maximum and minimum signature condition, respectively. Also, the minimum (5%) and maximum (95%) air temperature is computed based on sea temperature and ASTD, and the average (50%) ASTD is computed based on the annual mean sea and air temperature. These exceptions are also highlighted in blue in Table 2. Figures 9 and 11 show that the air temperature is above 0°C more than 90% of the time, and the ASTD is only positive (sea cooler than air) 30% of the time.

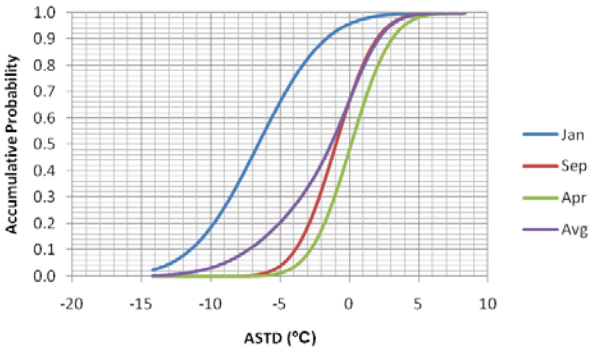

Figure 11: accumulative probabilities for air-sea temperature difference (ASTD).

4. INFRARED DETECTION

Figure 12 shows the main window of ShipIR/NTCS during a seeker engagement when the missile model takes control of the IR observer to simulate the target acquisition along a constant azimuth towards the ship. In this example, the seeker is oriented towards the sun-heated side of the untreated (dark-grey) destroyer, which is operating at full-power in the maximum daytime signature environment (es-jan). The FOV of the main window (800x600) is optimized for the user-specified seeker resolution (256x256 over 12°), and the dotted rectangle in the main window (512x512) shows the region being sampled by the seeker. The region of the main window containing the ship is also rendered full-image (800x600) using a special sub-image algorithm to maximize the spatial resolution of the target contrast signature. The three sub-windows to the right of the main window contain the raw seeker image (bottom), the line-by-line contrast image (middle), and the resultant detected pixels (top). Figure 13 contains magnified regions of the 3 sub-windows where the ship is located to show the ship contrast pixels being captured by the mid-wave sensor at a range of 13.1km and an altitude of 270m.

Table 2: scenario conditions spanning the range of min (5%), avg (50%) and max (95%) signature.

Signature:	Min	avg	max
Name:	es-aug	es-nov	es-jan
Month:	Aug	Oct	Jan
Tsea (°C):	25.5	14.5	5.2
Tair (°C):	28.4	12.9	-3.9
ASTD (°C):	2.9	-1.6	-9.1
DewPt (°C):	23.1	9.2	-5.4
Humidity (g/m^3):	20.55	8.87	3.29
RH (%):	74%	79%	90%
Wind (m/s):	7.66	6.24	5.02
Wind Dir. (°TN):	45°	315°	0°

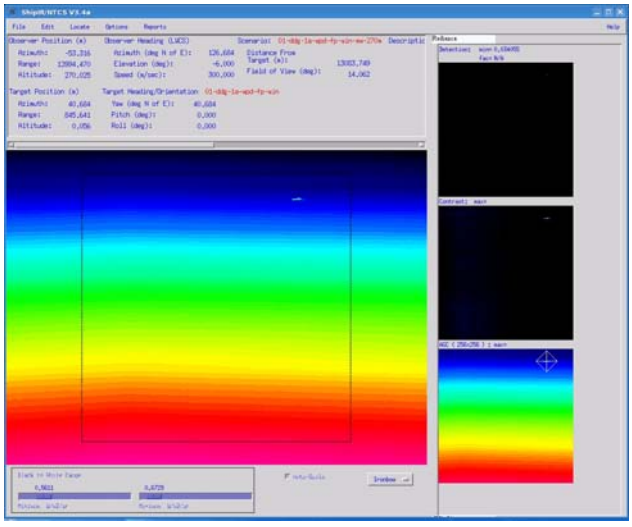

Figure 12: ShipIR/NTCS display during a seeker engagement.

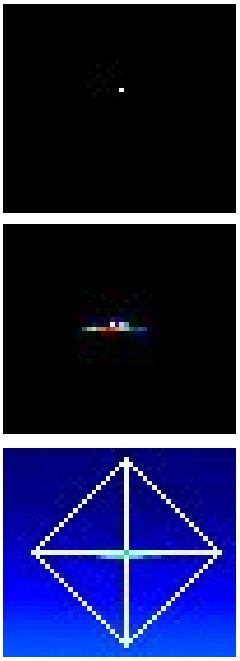

Figure 13: magnified areas of the seeker sub-windows.

The detection criteria used by the NTCS seeker model consist of the following: noise-equivalent radiance (NER) used to specify the noise level of the IR imaging system, the background clutter, or the line-by-line gradients in background signature, whichever is largest; a signal-to-noise ratio of SNR=5 corresponds to a Rose criterion of 100% probability of detection. A minimum no. of pixels (N_p) and consecutive frames (N_f) is also required to declare a lock-on. The noise-equivalent temperature differences (NETD) shown in Table 3 were obtained by comparing the residual seeker contrast signature (after the detection threshold is

applied) with the image analysis output from ShipIR for the same sensor trajectory. A series of contrast signature profiles are obtained for each value of NETD, as shown in Figure 14 for the LWIR sensor operating at an altitude of 10m in the maximum signature condition (es-jan). An NETD value of 0.3°C (lwir-3x) was chosen for this scenario. The two curves obtained from ShipIR image analysis, one using the same sensor FOV (Analysis) and the other using the LOOKAT command, shows that some of the ships contrast signature is a result of the sub-image algorithm. Testing may be required to determine if this algorithm can be further improved to minimize the effects of sub-imaging both the target and background within the sampling region.

Table 3: NETD values for each scenario.

Background	NETD (°C)			
	lw-010m	mw-010m	lw-270m	mw-270m
es-jan-clr	0.3	0.1	0.2	0.1
es-nov-clr	0.4	0.1	0.1	0.1
es-aug-clr	0.2	0.2	0.1	0.1
es-aug-cld	0.1	0.1	0.1	0.1

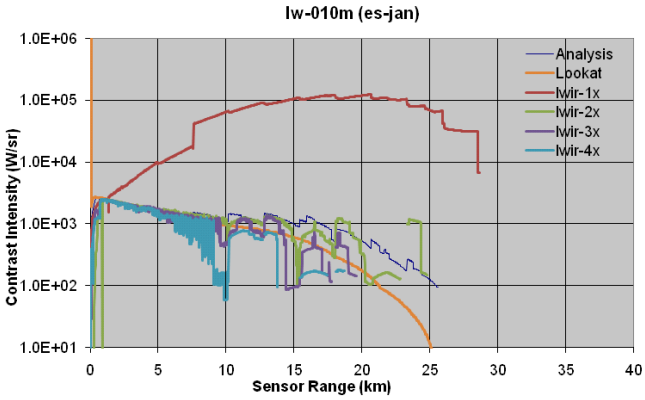

Figure 14; contrast signature versus range for different NETD.

5. ANALYSIS AND RESULTS

Figure 17 and 18 show the polar detection range from all four sensors against the unsuppressed and suppressed destroyer model, operating under average clear-day conditions (es-nov). Significant reductions are observed in three of the four sensors: LWIR at 10m, MWIR at 10m and 270m; minimal changes are observed in the lock range of the LWIR sensor at 270m, largely due to a negative air-sea temperature difference (ASTD=-1.6 °C). Further analysis of the MWIR fly-ins on the suppressed ship indicate the spikes in detection range are the result of sun-glint reflections off the ship surfaces, which could be removed from the analysis by increasing the no. of pixels and no. of frames required to declare a lock-on. These glint reflections have an equal likelihood not to occur due to ship motion and known irregularities in ship surface construction (these curvature effects are not included in the CAD model). A similar set of polar detection graphs are presented in Figure 15 and 16 for the same two ship configurations operated under minimum (clear-day) signature conditions (es-aug). More significant reductions are observed in the LWIR detection range from 270m due to the more favourable (+2.9°C) ASTD condition.

Over 400 scenarios were modelled and analysed, based on eight (4x2) backgrounds (min, max, and avg clear-sky, min overcast; day and night), four (4x) infrared sensors (MWIR and LWIR at 10m and 270m), three (3x) operating modes (quiet, cruise, full-power) and various signature treatments (LSA, stack suppression, hull film cooling). Scatter graphs and histograms of the detection range with and without infrared suppression are used to assess the overall IR susceptibility of the ship and quantify the effectiveness of each signature treatment, as illustrated by Figures 19 through 22 for the minimum for the minimum clear-day signature condition (es-aug). This paper summarizes the results and conclusions obtained from the analysis of these 400^{+} scenarios.

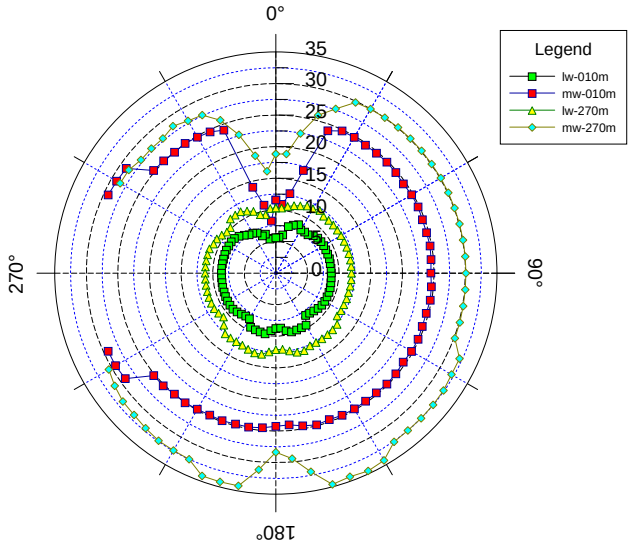

Figure 15: Detection range (km) of dark-grey destroyer at full-power with no signature treatment (best clear day).

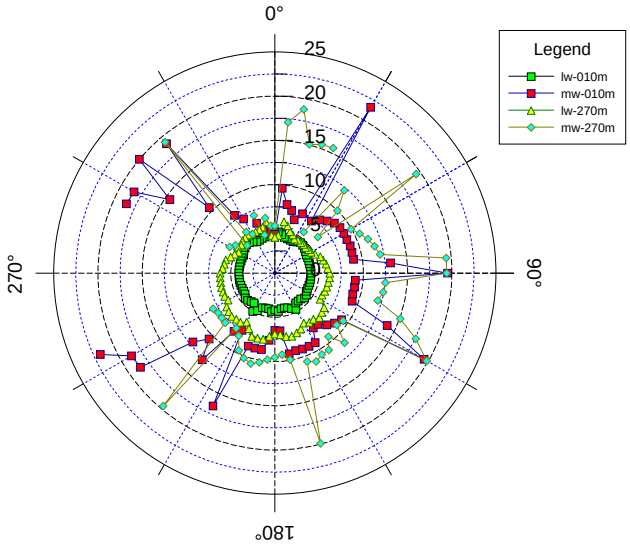

Figure 16: Detection range (km) of destroyer at full-power with stack suppression and hull film cooling (best clear day).

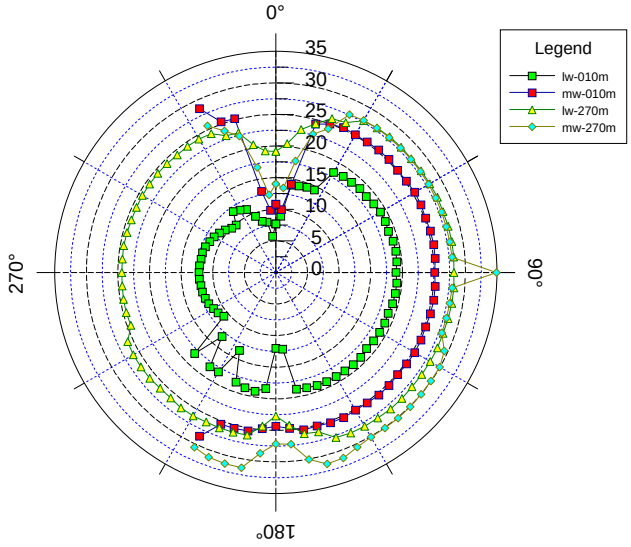

Figure 18: Detection range (km) of dark-grey destroyer at full-power with no signature reduction (average clear day).

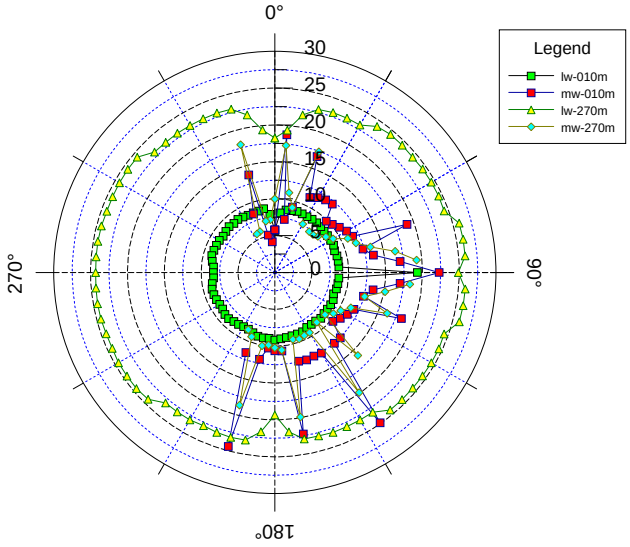

Figure 17 : Detection range (km) of destroyer at full-power with stack suppression and hull film cooling (average clear day).

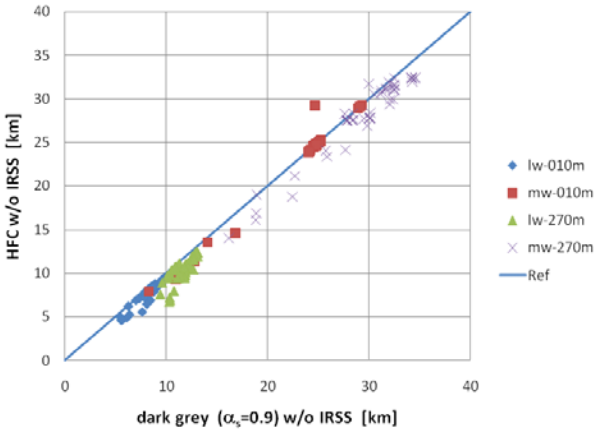

Figure 19: scatter diagram of the detection range with and without hull cooling (no stack suppression, min clear day).

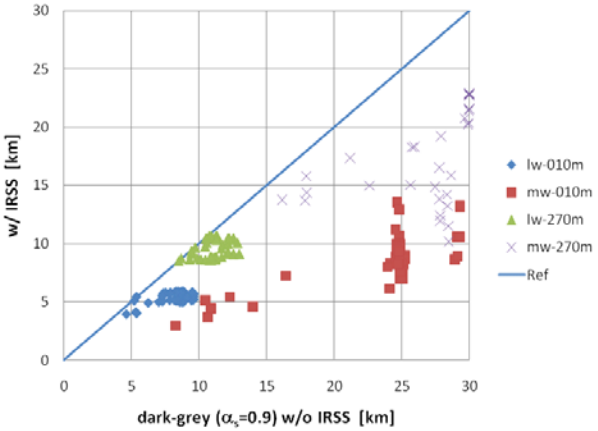

Figure 20: scatter diagram of the detection range with and without stack suppression (no hull cooling, min clear day).

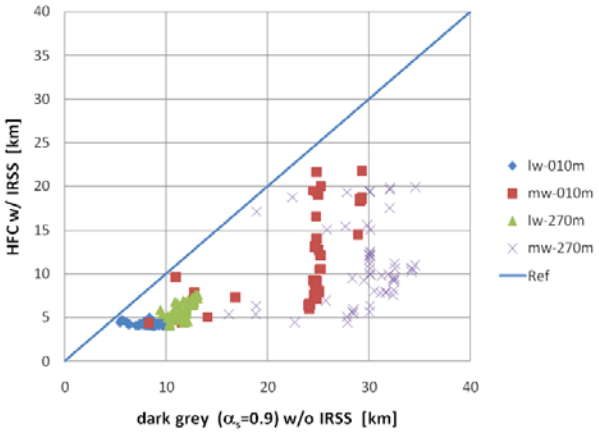

Figure 21: scatter diagram of the detection range with and without hull cooling and stack suppression (min clear day).

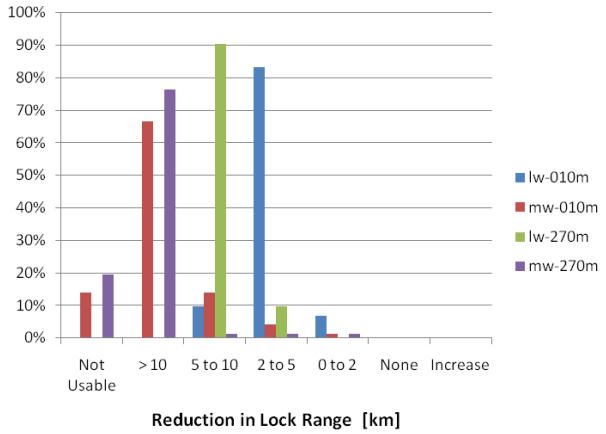

Figure 22: histogram of the reduction in detection range from hull cooling and stack suppression (min clear day).

6. SUMMARY AND CONCLUSION

In general, the IR susceptibility of the ship and the benefits of infrared suppression both increase with background thermal signature condition (min, avg, max) and engine power. The effectiveness of two available skin treatments (low solar absorptive paints, active hull cooling) are shown to increase with lower operating temperatures (air, sea, dew-point), but decrease with ship speed and engine power. The light-grey ship (α_s=0.50) produced a 0-30% lower average detection range than its dark-grey counterpart (α_s=0.90). Larger reductions in IR susceptibility are obtained using an active hull cooling system, with average decreases in detection ranging from 20-60%. The degradation in effectiveness of both skin treatments with engine power is related to the increased air convection (ambient cooling) and exhaust stack signature associated with increased ship speed. The effectiveness of the active hull cooling is also affected by one additional operating variable, the air-sea temperature difference (ASTD).

Reductions in IR signature and susceptibility associated with stack signature suppression tend to predominate the mid-wave band, with average decreases in detection ranging from 20-80%. Subsequently, the benefits are shown to decrease with lower engine power and lower ambient temperature and humidity, where the thermal skin signature tends to predominate.

Reductions in long-wave IR susceptibility are also apparent at night during cruise and full-power operations, where an average decrease in detection of 10-20% is observed.

A combination of both stack suppression and active hull cooling provides the maximum benefit with an average reduction in IR susceptibility ranging from 20-80%, depending on operating condition and engine speed. Since these two signature sources have a maximum detection in different regions of the operating spectrum (long-wave band skin signature at low engine power and ship speed, mid-wave stack signature at cruise and full-power), these two technologies complement each other and offer a wider operating envelope for the stealthy ship.

7. REFERENCES

1. Cox, C. and Munk, W., "Measurement of the Roughness of the Sea Surface from Photographs of the Sun's Glitter," *J. Opt. Society Am.* 44, 838-850 (1954).

2. Fraedrich, D., S., Stark, E., Heen, L.T., and Miller, C., "ShipIR model validation using NATO SIMVEX experiment results," *Proc. SPIE* 5075, Targets and Backgrounds IX: Characterization and Representation, 49-59 (2003).

3. Mermelstein, M., D., Shettle, E., P., Takken, E., H. and Priest, R., G., "Infrared radiance and solar glint at the ocean-sky horizon," *Appl. Opt.* 33 (25), 6022-6034 (1994).

4. Ross, V. and Dion, D., "Sea surface slope statistics derived from Sun glint radiance measurements and their apparent dependence on sensor elevation", J. Geophys. Res., 112, C09015, doi:10.1029/2007JC004137 (2007).

5. Shaw, J.A. and Churnsize, J.H., "Scanning-laser glint measurements of sea-surface slope statistics". *Appl. Opt.* 36 (18):4202-4213 (1997).

6. Vaitekunas, D., A. and Fraedrich, D., S., "Validation of the NATO-standard ship signature model (SHIPIR)," *Proc. SPIE* 3699, Targets and Backgrounds: Characterization and Representation V, 103-113 (1999).

7. Vaitekunas, D., A., "Technical Manual For ShipIR/NTCS (v2.9), Davis Document No. A912-002, Rev 0," (2002).

8. Vaitekunas, D., A, "Infrared Signature Instrumentation, Measurement, and Modelling of CFAV Quest for Trial Q276. Davis Document No. A320-001, Rev 0 (performed under PWGSC Contract No. W7707-3-2128)", 2004.

9. Vaitekunas, D., A., "Validation of ShipIR (v3.2): methods and results," 1st International Workshop for IR Target and Background Modelling 27–30 June Ettlingen Germany (2005).